Electronic Transactions on Numerical Analysis.
Volume 34, pp. 102-118, 2009.

ISSN 1068-9613.

ETNA
Kent State University
http://etna.math.kent.edu

HYBRID COMPACT-WENO SCHEME FOR SOLVING RELATIVISTIC FLOWS*

RICARD GARRIDO†, PEDRO GONZÁLEZ-CASANOVA‡, AND ELVIRA TORONDEL†

Dedicated to Víctor Pereyra on the occasion of his 70th birthday

Abstract. In this paper the method hybrid compact-WENO proposed by Yu-Xin Ren, Miao'er Liu and Hanxin Zhang has been modified to be used for relativistic fluid dynamics instead of Euler equations. The behavior of this new fifth-order conservative hybrid method is analyzed.

Key words. Hybrid compact-WENO, compact schemes, relativistic fluid dynamics, relativistic flows.

AMS subject classifications. 15A15, 15A09, 15A23

1. Introduction. Relativistic hydrodynamic simulations are more difficult than Newtonian simulations [11]. However, there has been much progress in relativistic numerical simulations during the last decade. We refer the reader to a comprehensive review of numerical relativistic hydrodynamics by Martí and Müller [10]. In this article, we investigate hybrid compact-WENO type schemes for solving relativistic flow problems. Compact schemes are very accurate in smooth regions with spectral resolution; see Lele [9]. However, it has been observed that they do produce non-physical oscillations when they are directly applied to flow with discontinuities. Moreover, it is well known that the non-physical oscillations (Gibbs phenomena) do not decay in magnitude when the grid is refined. In order to suppress the spurious oscillation and nonlinear instability, Cockburn and Shu [3] developed a nonlinear stable compact scheme for shock calculations.

An alternative approach is to develop so-called hybrid methods in which the non-oscillatory shock-capturing schemes are only used locally near discontinuities while compact schemes are used in smooth regions. The use of a conservative compact scheme not only facilitates the coupling with the WENO scheme, which is conservative by nature, but also makes the overall scheme conservative no matter which boundary closure scheme is adopted.

The hybrid compact-WENO scheme combines the advantages of compact schemes in smooth regions with the sharp WENO technique near the discontinuities. Another advantage of the hybrid methods is that they are computationally more efficient than other nonlinear compact schemes, since the computationally expensive non-oscillatory shock-capturing schemes are only used in regions containing the discontinuities.

The aim of this paper is to modify the hybrid compact-WENO, formulated in [13] for Eulerian flows, so that it can be applied to the equations of relativistic fluid dynamics (RFD). In order to achieve this objective, we first write these equations as a hyperbolic system of conservation laws, a task which is possible by choosing an appropriate vector of unknowns. Then, by using the spectral decomposition of the RFD system, we are able to formulate and modify the proposed numerical scheme.

It is worth to mentioning that recently Zhang et al. [15] proposed higher order extensions of the nonlinear weighted compact schemes and the weighted essentially nonoscillatory schemes of Jiang and Shu [8]. At the core of this contribution is the idea to directly interpolate the flux on its stencil instead of performing the nonlinear interpolation on the conservative

*Received March 29, 2008. Accepted November 5, 2008. Published online on August 25, 2009. Recommended by Godela Scherer.

†Departamento de Matemática Aplicada, Universidad de Valencia, CP.46100, Burjassot, Valencia, Spain (Ricard.Garrido@uv.es).

‡Unidad de Investigación en Cómputo Aplicado, DGSCA, Universidad Nacional Autónoma, Mexico, (pedrogc@dgsca2.unam.mx,eltolo@alumni.uv.es).

ETNA
Kent State University
http://etna.math.kent.edu

variables as in Deng and Zhang [4]. Since the authors report that this approach has the same ability to capture strong discontinuities, while the resolution of short waves is improved and numerical dissipation is reduced, it may have an interesting impact in the solution of the relativistic fluid dynamics equations analyzed in this work.

This article is organized as follows. In Section 2, the relativistic fluid dynamics equations are introduced. In Section 3, the compact-WENO method is described in general (Section 3.1) and its adaptation to RFD (Section 3.3) is discussed. In particular, the parameter which determines the behavior of the hybrid scheme is reformulated and discussed in Section 3.2. In Section 4, the results of several numerical experiments in 1D and 2D are presented in order to compare hybrid compact-WENO with WENO schemes. Section 5 contains final remarks and conclusions.

2. Relativistic fluid dynamics. In general, a relativistic fluid is characterized by phenomena which involve gas moving at velocities close to the speed of light. In this context, relativistic equations have to be used instead of the Euler equations for fluid dynamics.

Within the framework of restricted relativity, a relativistic flux is described by a system of equations of local conservation laws, given by

$$\nabla_\mu(\rho U^\mu) = 0 \qquad \text{local conservation of the baryonic number density,} \tag{2.1}$$

$$\nabla_\mu T^{\mu\nu} = 0 \qquad \text{local conservation of the momentum-energy tensor.} \tag{2.2}$$

Throughout this section, Greek indices run from 0 to 3, and Latin indices from 1 to 3. In the former equations, ρ is the rest mass density, U^μ the 4-velocity vector and ∇_μ stands for the covariant derivative. $T^{\mu\nu}$ is the energy-momentum tensor, which for a perfect fluid can be written as

$$T^{\mu\nu} = \rho h u_\mu u_\nu + p g_{\mu\nu}, \tag{2.3}$$

where p is the pressure and $h = 1 + \epsilon + p/\rho$ is the specific enthalpy, with ϵ being the specific internal energy. The tensor $g_{\mu\nu}$ defines the metric of the space-time where the fluid evolves.

The first step to build the hybrid numerical scheme consists in rewriting (2.1) and (2.2) in conservative form, see (2.11). To do so, we recall from [5] that the system of equations (2.1) and (2.2) can be rewritten as

$$\frac{\partial F^\mu(w)}{\partial x^\mu} = 0 \tag{2.4}$$

with

$$w = (\rho, v^i, \epsilon)^T, \tag{2.5}$$

$$F^0(w) = (\rho W, \rho h W^2 v^j, \rho h W^2 - p - \rho W)^T, \tag{2.6}$$

$$F^i(w) = (\rho W v^i, \rho h W^2 v^j v^i + p\delta^{ij}, \rho h W^2 v^i - \rho W v^i)^T, \tag{2.7}$$

where $x^\mu = (t, x, y, z)$; and $v^i = u^i/W$, where W is the Lorentz factor which satisfies $W = (1 - v^2)^{-1/2}$, with $v^2 = \delta_{ij} v^i u^j$.

Consider now the variables

$$\begin{cases} D = \rho W \\ S^j = \rho h W^2 v^j \\ \tau = \rho h W^2 - p - \rho W, \end{cases} \tag{2.8}$$

ETNA
Kent State University
http://etna.math.kent.edu

which are, respectively, the rest mass, momentum, and total energy densities, measured in the laboratory frame. Defining now the conserved quantities

$$u = (D, S^j, \tau)^T \tag{2.9}$$

$$f^i(u) = \left(Dv^i, S^j v^i + p\delta^{ij}, S^i - Dv^i\right)^T, \tag{2.10}$$

the system takes the form

$$\frac{\partial u}{\partial t} + \sum_i \frac{\partial f^i}{\partial x_i} = 0, \tag{2.11}$$

which is the desired conservative representation. The system is closed with an equation of state $p = p(\rho, \epsilon)$ and is hyperbolic for causal equations of state; see Anile [2]. The solution of hyperbolic non-linear systems of conservation laws by means of component-wise or characteristic-wise type schemes requires as a first step the spectral decomposition of the system. In these schemes, the characteristic structure is used to compute the local characteristic fields, which define the directions along which the characteristic variables propagate. The full spectral decomposition of the three 5×5 Jacobian matrices B^i associated with the system (2.11),

$$\mathcal{B}^i = \frac{\partial f^i(u)}{\partial u}, \tag{2.12}$$

which is at the very core of this paper, can be found in Donat et al. [5]. For completeness, we include the expressions of the eigenvalues

$$\lambda_0 = v^x \qquad \text{(triple)}, \tag{2.13}$$

which define the material waves, and

$$\lambda_\pm = \frac{1}{1 - v^2 c_s^2}\left\{v^x(1 - c_s^2) \pm c_s\sqrt{(1 - v^2)[1 - v^x v^x - (v^2 - v^x v^x)c_s^2]}\right\}, \tag{2.14}$$

which are associated to the acoustic waves. Note that the characteristic wave speeds in the relativistic case not only depend on the fluid velocity components in the wave propagation direction, but also on the normal velocity components. This coupling adds new numerical difficulties which are specific to relativistic fluid dynamics; see Ibañez [7].

In what follows, for simplicity of exposition and since its extension to several dimensions is straightforward, we shall present the component-wise algorithm in one dimension. In this case, the Jacobian matrix of (2.12) has three real and distinct eigenvalues, one associated with material waves and two with acoustic waves: v and $(v \pm c_s)/(1 \pm v c_s)$.

Although component-wise methods are simple and cost effective [14], for more demanding test problems, it is advisable to use the more costly, but much more robust, characteristic decomposition. The combination of spectral methods with characteristic-type schemes is thus expected to produce more precise results at a lower cost.

3. Compact-WENO scheme. In this section, we first describe in general the compact-WENO method and we discuss how to adapt this technique to the RFD problem. In particular, we discuss and reformulate the parameter which determines the behavior of the hybrid scheme in such a way that it can accurately solve the RFD problem.

ETNA
Kent State University
http://etna.math.kent.edu

3.1. The finite difference equation. Consider the scalar hyperbolic conservation law

$$\frac{\partial u}{\partial t} + \frac{\partial f}{\partial x} = 0 \qquad \text{where } f = f(u). \tag{3.1}$$

$\frac{\partial f}{\partial u}$ is a real function of u. Let $\{I_j\}$ be a uniform partition of the solution domain in space, where $I_j = [x_{j-1/2}, x_{j+1/2}]$ and $x_{j+1/2} - x_{j-1/2} = h$.

The semi-discrete conservative finite difference scheme of (3.1) can be written as

$$\frac{\partial u_j}{\partial t} + \frac{1}{h}\left(\hat{f}_{j+1/2} - \hat{f}_{j-1/2}\right) = 0, \tag{3.2}$$

where $\hat{f}_{j+1/2}(u_{j-k}, ..., u_{j+k+1})$ is a numerical flux function such that

$$\frac{1}{h}\left(\hat{f}_{j+1/2} - \hat{f}_{j-1/2}\right) = \left(\frac{\partial f}{\partial x}\right)_j + O(h^k), \tag{3.3}$$

which implies that the scheme is kth order accurate in space.

The time integration will be performed by means of a three-stage, TVD Runge-Kutta scheme. Defining

$$L_j(u) = -\frac{1}{h}\left(\hat{f}_{j+1/2} - \hat{f}_{j-1/2}\right), \tag{3.4}$$

the TVD Runge-Kutta scheme is given by

$$u_j^{(1)} = u_j^n + \Delta t L_j(u^n), \tag{3.5}$$

$$u_j^{(2)} = \frac{3}{4}u_j^n + \frac{1}{4}u_j^{(1)} + \frac{1}{4}\Delta t L_j(u^{(1)}), \tag{3.6}$$

$$u_j^{n+1} = \frac{1}{3}u_j^n + \frac{2}{3}u_j^{(2)} + \frac{2}{3}\Delta t L_j(u^{(2)}). \tag{3.7}$$

This scalar numerical technique is at the core of the characteristic-wise algorithm used to solve systems of equations, where at each point we project the variables and the fluxes onto the local characteristic space. In terms of these characteristic fields, the equations locally decouple, and we are in a position to apply the scheme separately to each of the characteristic fields. The specific numerical fluxes that we shall use in this article will be explained in the following section.

3.2. The hybrid compact-WENO scheme. As we mentioned above, compact schemes give very satisfactory results if the solution is smooth everywhere. However, Gibbs phenomena will occur when there are discontinuities in the solution. Gibbs phenomena will contaminate the solution and may lead to nonlinear instabilities. In order to cure this deficiency a hybrid compact-WENO method was proposed in [1, 12] in which the compact scheme is coupled with an ENO or a WENO scheme. As a result, the proposed hybrid method uses the compact scheme segment by segment in smooth regions, while near the discontinuities that separate the smooth regions, the ENO/WENO scheme is used instead.

The hybrid scheme presented here appears in [13] and is constructed by considering the weighted average of two sub-schemes: the conservative upwind compact scheme of fifth order and the WENO scheme.

The system can be written as follows

$$\sigma_{j+1/2}\phi_{j+1/2}\hat{f}_{j-1/2} + \hat{f}_{j+1/2} + \sigma_{j+1/2}\psi_{j+1/2}\hat{f}_{j+3/2} = \hat{c}_{j+1/2}, \tag{3.8}$$

ETNA
Kent State University
http://etna.math.kent.edu

where

$$\phi_{j+1/2} = \frac{1}{3} + \frac{s_{j+1/2}}{6}, \qquad \psi_{j+1/2} = \frac{1}{3} - \frac{s_{j+1/2}}{6}, \tag{3.9}$$

$$s_{j+1/2} = \operatorname{sign}(\tilde{a}_{j+1/2}) \tag{3.10}$$

$$\tilde{a}_{j+1/2} = \begin{cases} \frac{\hat{f}_{j+1} - \hat{f}_j}{u_{j+1} - u_j} & \text{if } u_{j+1} - u_j \neq 0, \\ \left(\frac{\partial f}{\partial u}\right)_j, & \text{otherwise,} \end{cases} \tag{3.11}$$

$$\hat{c}_{j+1/2} = \sigma_{j+1/2}\hat{b}_{j+1/2} + (1 - \sigma_{j+1/2})\hat{f}^{\mathrm{WENO}}_{j+1/2} \tag{3.12}$$

$$\begin{aligned} \hat{b}_{j+1/2} = {} & \left(\frac{1 - s_{j+1/2}}{2}\right)\left(\frac{1}{18}f_{j-1} + \frac{19}{18}f_j + \frac{5}{9}f_{j+1}\right) + \\ & \left(\frac{1 - s_{j+1/2}}{2}\right)\left(\frac{5}{9}f_j + \frac{19}{18}f_{j+1} + \frac{1}{18}f_{j+2}\right) \end{aligned} \tag{3.13}$$

$$\hat{f}^{\mathrm{WENO}}_{j+1/2} = \sum_{\gamma=0}^{2} \omega_\gamma f^\gamma_{j+1/2}, \tag{3.14}$$

and $\sigma_{j+1/2}$ is a weight which is directly related to the smoothness of the numerical solution. In equation (3.14), $f^\gamma_{j+1/2}$ is obtained by a second order polynomial reconstruction of $f(u(x_{x_j+1/2}))$ on the γth set candidate stencils S_γ. For each γ, the weight ω_γ satisfies the condition $\omega_\gamma > 0$, $\sum_\gamma \omega_\gamma = 1$; see Procedure 2.5 in [14] for more details. In this numerical scheme, a smoothness indicator $r_{j+1/2}$ is defined and the weight should be a function of $r_{j+1/2}$.

In the present paper, the smoothness indicator is designed to be

$$r_{j+1/2} = \min(r_j, r_{j+1}), \tag{3.15}$$

where

$$r_j = \frac{|2\Delta f_{j+1/2}\Delta f_{j-1/2}| + \varepsilon}{(\Delta f_{j+1/2})^2 + (\Delta f_{j-1/2})^2 + \varepsilon} \tag{3.16}$$

and $\Delta f_{j+1/2} = f_{j+1} - f_j$; $\varepsilon = \frac{0.9\tilde{r}_c}{1-0.9\tilde{r}_c}\zeta^2$ is a positive real number to avoid possible division by zero. Here, ζ is a user-specified positive number which will be explained in the next subsection.

To make a compromise between the robustness, the efficiency, and the accuracy of the method, it is suggested in [13] that the weight should be a continuous rather than a smooth function of the smoothness indicator. Under these conditions, the weight takes the following form

$$\sigma_{j+1/2} = \min\left(1, \frac{r_{j+1/2}}{\tilde{r}_c}\right), \tag{3.17}$$

where $\tilde{r}_c$ is a threshold value which is usually problem-dependent.

3.2.1. Choice of $\tilde{r}_c$. Suppose that ε is small enough so that it can be ignored in (3.16) and let $x = \Delta f_{j-1/2}$ and $y = \Delta f_{j+1/2}$. Then we have

$$r_j = \frac{2|x||y|}{x^2 + y^2} = 2\frac{|x|}{\sqrt{x^2+y^2}}\frac{|y|}{\sqrt{x^2+y^2}} = 2\sin\theta\cos\theta = \sin(2\theta) \quad \text{where} \quad \theta \in [0, \pi/2].$$

ETNA
Kent State University
http://etna.math.kent.edu

We are interested in finding the values of θ which determine under which circumstances the WENO scheme is not used. This happens when (see (3.17))

$$\frac{r_j}{\tilde{r}_c} \geq 1; \qquad \text{that is,} \qquad \frac{\sin(2\theta)}{\tilde{r}_c} \geq 1 \Rightarrow \sin(2\theta) \geq \tilde{r}_c. \tag{3.18}$$

The threshold values of this relation are $\theta_1 \in [0, \pi/4]$ and $\theta_2 \in [\pi/4, \pi/2]$, so that for all $\theta \in [\theta_1, \theta_2]$, the WENO scheme is not used. Recall that (3.18) is equivalent to $\tan(2\theta) \geq \tilde{r}_c(\theta)$, which provides an explicit relation between $\tilde{r}_c$ and $\tan(2\theta)$.

Considering now that $z_1 = \tan(\theta_1)$ and $z_2 = \tan(\theta_2)$, and noting that $|\frac{x}{y}| = \tan(\theta)$, we do not have to calculate a WENO scheme for all $|\frac{x}{y}| \in [z_1, z_2]$, which gives a geometrical interpretation of the $\tilde{r}_c$ parameter. On the other hand, when the value $|\frac{x}{y}|$ is too big or too small due to the presence of non-smooth data, the WENO scheme is replaced by the compact method.

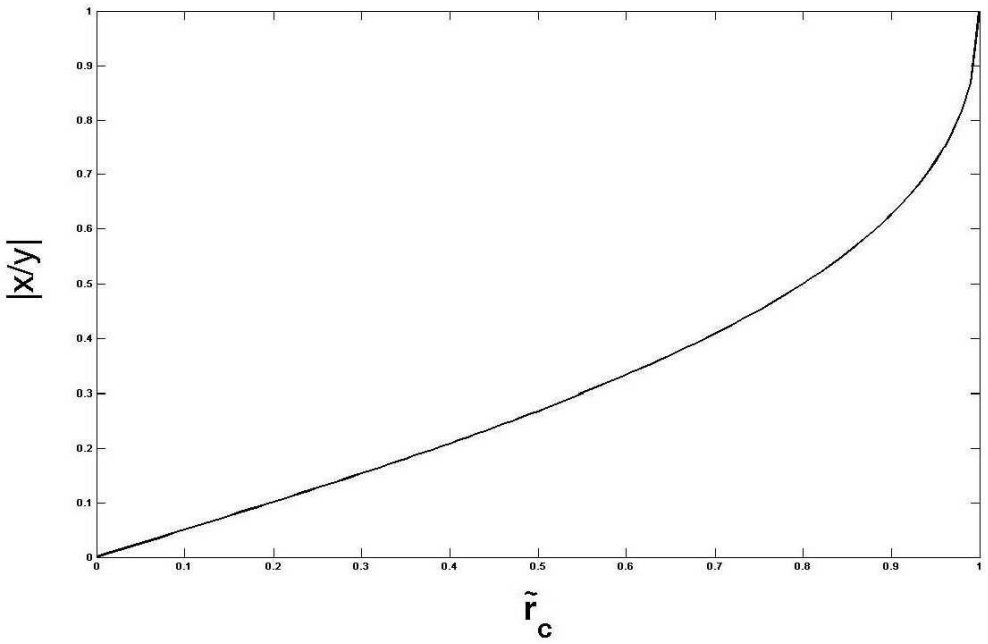

FIGURE 3.1. *Relation between* $|\frac{x}{y}|$ *and* $\tilde{r}_c$.

As we can see in Figure 3.1, for small values of $\tilde{r}_c$ the relation of $|\frac{x}{y}|$ with $\tilde{r}_c$ is almost linear. Under these circumstances, numerical experiments have shown that the quality of the solution is not very sensitive to changes of the $\tilde{r}_c$ parameter. This can be explained as a result of this linear behavior.

In turbulent fluxes, it has been proved that compact schemes resolve the fluctuations better than a finite difference scheme such as WENO, so it is required that the hybrid scheme uses a compact method when such zones appear. The parameter ε is used to recognize these turbulent fluxes. When small but strong fluctuations are found in the numerical solution, the term ε dominates and $\sigma_{j+1/2} \approx 1$, so the scheme will be purely compact. Indeed, when $\max\left(|\Delta f_{j-1/2}|, |\Delta f_{j+1/2}|, |\Delta f_{j+3/2}|\right) < \zeta$ then $\sigma_{j+1/2} > 0.9$. Note that ζ acts as a threshold value, such that all fluctuations smaller than this value will be considered as turbulent fluctuations and consequently will not be damped by using WENO [13].

ETNA
Kent State University
http://etna.math.kent.edu

Numerical experiments have shown that the numerical solution is less sensitive to strong changes in ζ; thus, we will keep $\zeta = 10^{-3}$ in all our numerical experiments, as proposed in [13].

3.3. Compact-WENO scheme for RFD. As mentioned in Section 2, and since its extension to several dimensions is straightforward, we shall here present the hybrid scheme for relativistic flows in one dimension only. When solving the RFD equations the evaluation of the numerical flux functions for the characteristic-wise hybrid compact-WENO scheme can be obtained by the following steps:

1. At each fixed $x_{j+1/2}$, the average state $u_{j+1/2}$ is computed by the simple mean
$$u_{j+1/2} = \frac{1}{2}(u_j + u_{j+1}). \tag{3.19}$$
2. The eigenvalues $\lambda^{(i)}_{j+1/2}$ $(i = 1, 2, 3)$ and the left eigenvectors $l^{(i)}_{j+1/2}$ $(i = 1, 2, 3)$ are computed in terms of $u_{j+1/2}$.
3. The local characteristic decompositions of the flux functions at x_m for $m = j - 1, ..., j + 2$ are computed by using
$$w^{(i)}_m = l^{(i)}_{j+1/2} f_m, \qquad i = 1, 2, 3, \quad m = j - 1, \ldots, j + 2. \tag{3.20}$$
4. Define
$$\begin{aligned}
s^{(i)}_{j+1/2} &= \operatorname{sign}\left(\lambda^{(i)}_{j+1/2}\right), \\
r^{(i)}_{j+1/2} &= \min\left(r^{(i)}_j, r^{(i)}_{j+1}\right), \\
r^{(i)}_j &= \frac{|2\Delta w^{(i)}_{j+1/2}\Delta w^{(i)}_{j-1/2}| + \varepsilon}{(\Delta w^{(i)}_{j+1/2})^2 + (\Delta w^{(i)}_{j-1/2})^2 + \varepsilon}, \\
\sigma^{(i)}_{j+1/2} &= \min\left(1, \frac{r^{(i)}_{j+1/2}}{\tilde{r}_c}\right), \\
\sigma_{j+1/2} &= \min_{(i)}\left(\sigma^{(i)}_{j+1/2}\right).
\end{aligned}$$

Note that $\sigma_{j+1/2}$ has been modified from the original formula used in [13]. This change is due to the presence of negative pressures which appear when using the formulation given in [13]. Moreover, the motivation for changing this term is the fact that by using the original formula given in [13], the corresponding matrix of (3.23) becomes extremely ill-conditioned due the height differences between the values of the relativistic eigenvectors.

As can be seen from equation (3.12), if $\sigma^{(i)}_{j+1/2} = 0$, this implies that the scheme only uses the WENO method in the corresponding (i) component. Recall that in our problem, we have only one of the (i) components different from zero while the rest are zero. Then the structure of (3.24) and (3.26) is affected due to strong coupling. With the choice of $\sigma_{j+1/2} = \min_{(i)}\left(\sigma^{(i)}_{j+1/2}\right)$ we aim to unify the behavior of the method for the (i) components in such way that the WENO technique will be used whenever any of the (i) components uses WENO. In this case, we can guarantee that uniform blocks will be produced.

ETNA
Kent State University
http://etna.math.kent.edu

For $i = 1, 2$, and 3, the hybrid compact-WENO scheme for the scalar equation (3.8) can be applied to the local characteristic variables $w^{(i)}$ $(i = 1, 2, 3)$ by means of the following system of equations

$$\sigma_{j+1/2}\phi^{(i)}_{j+1/2}\hat{w}^{(i)}_{j-1/2} + \hat{w}^{(i)}_{j+1/2} + \sigma_{j+1/2}\psi^{(i)}_{j+1/2}\hat{w}^{(i)}_{j+3/2} = \hat{c}^{(i)}_{j+1/2}, \tag{3.21}$$

where

$$\phi^{(i)}_{j+1/2} = \frac{1}{3} + \frac{s^{(i)}_{j+1/2}}{6}, \qquad \psi^{(i)}_{j+1/2} = \frac{1}{3} - \frac{s^{(i)}_{j+1/2}}{6},$$

$$\hat{c}^{(i)}_{j+1/2} = \sigma^{(i)}_{j+1/2}\hat{b}^{(i)}_{j+1/2} + (1 - \sigma^{(i)}_{j+1/2})\tilde{w}^{(i),\mathrm{WENO}}_{j+1/2}, \tag{3.22}$$

and

$$\hat{b}^{(i)}_{j+1/2} = \left(\frac{1 + s^{(i)}_{j+1/2}}{2}\right)\left(\frac{1}{18}w^{(i)}_{j-1} + \frac{19}{18}w^{(i)}_{j} + \frac{5}{9}w^{(i)}_{j+1}\right) + \left(\frac{1 - s^{(i)}_{j+1/2}}{2}\right)\left(\frac{5}{9}w^{(i)}_{j} + \frac{19}{18}w^{(i)}_{j+1} + \frac{1}{18}w^{(i)}_{j+2}\right).$$

It should be noted that for fixed i, (3.21) cannot be solved directly since the $\hat{w}^{(i)}_{j+1/2}$ is defined locally in terms of the characteristic variables $w^{(i)}_m$; see (3.3). Consequently, in the following step, (3.21) for all characteristic fields will be arranged into a block-tridiagonal system of equations that can be solved to obtain the numerical flux in the physical space.

5. For $i = 1, 2, 3$, equation (3.21) can be written as

$$\Phi_{j+1/2}\hat{f}_{j-1/2} + L_{j+1/2}\hat{f}_{j+1/2} + \Psi_{j+1/2}\hat{f}_{j+3/2} = \hat{c}_{j+1/2}, \tag{3.23}$$

where

$$\Phi_{j+1/2} = \begin{bmatrix} \sigma^{(1)}_{j+1/2}\phi^{(1)}_{j+1/2}l^{(1)}_{j+1/2} \\ \sigma^{(2)}_{j+1/2}\phi^{(2)}_{j+1/2}l^{(2)}_{j+1/2} \\ \sigma^{(3)}_{j+1/2}\phi^{(3)}_{j+1/2}l^{(3)}_{j+1/2} \end{bmatrix}, \tag{3.24}$$

$$L_{j+1/2} = \begin{bmatrix} l^{(1)}_{j+1/2} \\ l^{(2)}_{j+1/2} \\ l^{(3)}_{j+1/2} \end{bmatrix}, \tag{3.25}$$

$$\Psi_{j+1/2} = \begin{bmatrix} \sigma^{(1)}_{j+1/2}\psi^{(1)}_{j+1/2}l^{(1)}_{j+1/2} \\ \sigma^{(2)}_{j+1/2}\psi^{(2)}_{j+1/2}l^{(2)}_{j+1/2} \\ \sigma^{(3)}_{j+1/2}\psi^{(3)}_{j+1/2}l^{(3)}_{j+1/2} \end{bmatrix}, \tag{3.26}$$

$$\hat{c}_{j+1/2} = \begin{bmatrix} \hat{c}^{(1)}_{j+1/2} \\ \hat{c}^{(2)}_{j+1/2} \\ \hat{c}^{(3)}_{j+1/2} \end{bmatrix}. \tag{3.27}$$

ETNA
Kent State University
http://etna.math.kent.edu

4. Numerical tests. Our intention is to prove that the hybrid compact-WENO scheme provides a better representation for shortened length scales than the one obtained when we use only the WENO scheme. As mentioned, this behavior is expected because compact schemes are very accurate in smooth regions with spectral-like resolution for problems which present a large range of scales.

In what follows, we study three problems in 1D and two problems in 2D in order to investigate the advantages of the hybrid compact-WENO method. Boundary conditions are set by filling the data in guard or ghost cells. The computational grid is extended on each side of the physical domain to compute the fluxes at the interfaces. In this paper, we have used both absorbent and prescribed boundary conditions. These boundary conditions have to be provided at each time step for all primitive and conservative variables.

For comparison purposes, we first build a reference simulation against which we will compare every result. This solution is built by means of a WENO5 method with Lax-Friedrich flux splitting coupled with a TVD-RK3 in a grid of 10000 points for 1D and 1000×1000 for 2D, with $\frac{\Delta t}{\Delta x} = 0.8$ for 1D and $\frac{\Delta t}{\Delta x} = 0.5$ for 2D at a final time $T = 0.4$ for 1D and $T = 0.8$ for 2D.

In 1D, we start testing the algorithm with a smooth 1D hydrodynamical solution which has been recently studied numerically in [6], for different methods. The second problem to be analyzed is a shock tube with non-oscillatory initial condition, whereas the third problem has a turbulent right initial condition.

In 2D, the numerical experiments will be performed on the square $[0,1]^2$, having a uniformly distributed gas with $\Gamma = \frac{5}{3}$, and $\rho = 10, v = 0, p = 13.3$. At $t = 0$, we start to feed the square with a gas determined by the data $\rho = 10, v_x = 0, v_y = 0.9c, p = 13.3$ and $\rho = 10, v_x = 0, v_y = 0.99c, p = 13.3$ for the first and second problem respectively, for the region $0.4 < x < 0.6, y = 0$, while other boundary conditions are set to be absorbent.

4.1. 1D. PROBLEM 4.1. In this problem, we focus on the case of a varying density profile $\rho = \rho(x,t)$ with constant, uniform pressure $p = p_0$ and velocity $v = v_0$. When these functions are substituted into (2.11), we see that they form a consistent solution for the advection of a density profile at constant velocity v_0. This test is performed on the computational domain $0 \leq x \leq 1$ for an ideal gas with $\Gamma = 5/3$. We consider two sets of initial conditions for this problem. The first initial conditions are given by

$$\{p = 1.0, \rho = \sin(32\pi x) + 2, v = 0.4\} \qquad x \in [0,1] \tag{4.1}$$

and the second initial conditions are

$$\{p = 1.0, \rho = \sin(2\pi x) + 2, v = 0.4\} \qquad x \in [0,1]. \tag{4.2}$$

In both cases, we have two smooth analytic solutions which behave as stationary traveling waves. The solution (4.1), which presents more oscillations, is designed to prove the effectiveness of the hybrid scheme when the parameter r_c is varied, while the second solution (4.2) is built to verify the order of convergence of the hybrid scheme. The corresponding results are shown in Tables 4.1 and 4.2. As can be appreciated from Table 4.1, for small values of $\tilde{r}_c$, the hybrid scheme not only gives a better error, but also a smaller CPU time. Thus, we verify that the hybrid scheme has superior performance to the pure WENO method for this case. This behavior is consistent with the fact that compact schemes are better suited for the approximation of smooth oscillatory solutions. The challenge, which is the subject of the following cases, is whether this improvement holds for highly non-smooth relativistic solutions. On the other hand, in Table 4.2, we can see that the order of convergence of the hybrid

ETNA
Kent State University
http://etna.math.kent.edu

method is consistent with the third-order Runge Kutta time integration technique.

PROBLEM 4.2. The initial conditions for the second problem are

$$\{p_L = 13.3, \rho_L = 10, v_L = 0\} \qquad x \in [0, 0.5[, \tag{4.3}$$

$$\{p_R = 0, \rho_R = 1, v_R = 0\} \qquad x \in [0.5, 1]. \tag{4.4}$$

The results are shown in Tables 4.3 and 4.4.

TABLE 4.1
Hybrid and WENO schemes for problem 1; initial conditions: (4.1), with $N = 200$ points, $T = 2.5$, $\frac{\Delta t}{\Delta x} = 0.8$.

HYBRID	$\tilde{r}_c$	CPU-Time (s)	$\|\|\|_2$	% WENO
	0.1	11.0	0.0898	4.82
	0.3	11.0	0.0884	15.22
	0.5	12.0	0.0900	28.16
	0.7	13.0	0.0960	47.17
	0.9	13.0	0.1116	70.52
WENO	–	14.0	0.1348	100

TABLE 4.2
Hybrid scheme for problem 1; initial conditions: (4.1), with $\tilde{r}_c = 0.1$, $T = 2.5$, $\frac{\Delta t}{\Delta x} = 0.5$.

npts	$\|\|\|_2$	CPU-Time (s)	% WENO
25	0.08144	0.0	2.81
50	0.04406	0.0	1.40
100	0.02619	3.0	0.40
200	0.01741	9.0	0.01
400	0.01277	78.0	0.0
800	0.01073	345	0.0

TABLE 4.3
Schemes: Hybrid and WENO for problem 2 in 1D with $N = 625$ points, $T = 0.4$, $\frac{\Delta t}{\Delta x} = 0.8$.

HYBRID	$\tilde{r}_c$	CPU-Time (s)	$\|\|\|_2$	$\|\|\|_\infty$	Local error	% WENO
	0.1	–	–	–	–	–
	0.15	38.187	0.0891	1.4349	0.2668	4.43
	0.2	38.046	0.0938	1.6113	0.2617	5.05
	0.3	38.046	0.1003	1.7615	0.2775	5.52
	0.4	38.030	0.1042	1.8361	0.2896	5.70
	0.5	38.483	0.1054	1.8568	0.2943	6.01
	0.6	38.436	0.1065	1.8777	0.2978	6.39
	0.7	38.577	0.1075	1.8931	0.3016	7.05
WENO	–	43.7	0.1156	2.0125	0.3300	100

We can see from the results of Tables 4.3 and 4.4 that the new definition $\sigma_{j+1/2} = \min_{(i)} \left(\sigma^{(i)}_{j+1/2}\right)$ works well. In this case the behavior of the two algorithms are quite similar. However, as we can see in Tables 4.3 and 4.4, the error produced by the hybrid method is better than corresponding error of the WENO technique.

Recall that the choice of the parameter $\tilde{r}_c$ corresponds to % of use of WENO. Thus, the larger the parameter is, the more the WENO scheme will be used. So it is not difficult

ETNA
Kent State University
http://etna.math.kent.edu

TABLE 4.4
Schemes: Hybrid and WENO for problem 2 in 1D with $N = 1250$ points, $T = 0.4$, $\frac{\Delta t}{\Delta x} = 0.8$.

HYBRID	$\tilde{r}_c$	CPU-Time (s)	$\|\|\|_2$	$\|\|\|_\infty$	Local error	% WENO
	0.1	–	–	–	–	–
	0.15	160.264	0.0511	0.9495	0.1492	1.83
	0.2	154.140	0.0485	0.9030	0.1289	2.14
	0.3	153.203	0.0486	0.8124	0.1390	2.50
	0.4	153.421	0.0499	0.8768	0.1509	2.64
	0.5	153.812	0.0511	0.9243	0.1594	2.86
	0.6	160.327	0.0516	0.9446	0.1637	3.16
WENO	–	172	0.0586	1.0707	0.1989	100

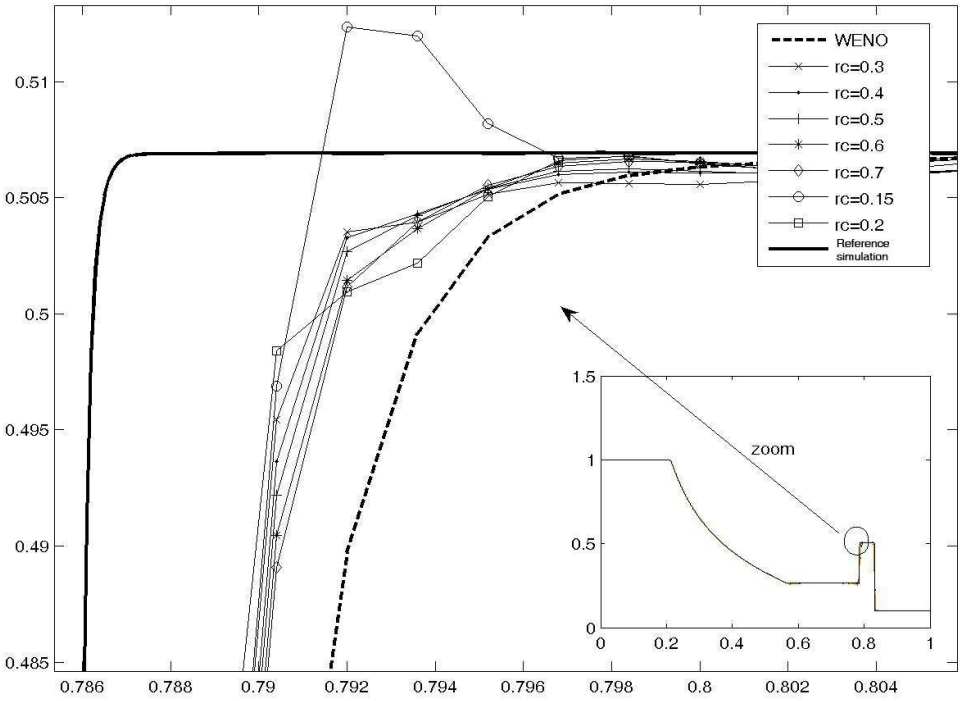

FIGURE 4.1. *Several $\tilde{r}_c$ for problem 2 with 625 points.*

to notice that the smaller $\tilde{r}_c$, the more oscillatory (near discontinuities) the solution will be, because the WENO is less used; see Figures 4.1 and 4.2.

PROBLEM 4.3. The third initial value problem is

$$\{D(x) = 10, S(x) = 0, \tau(x) = 19.95\}_L \qquad x \in [0, 0.5[, \tag{4.5}$$

$$\{D(x) = 1 + 0.2 \cdot \sin(20\pi x), S(x) = 0, \tau(x) = 9.9 \cdot 10^{-7}\}_R \qquad x \in [0.5, 1]. \tag{4.6}$$

As we can see in Tables 4.5 and 4.6, the hybrid compact-WENO scheme has smaller error and smaller execution time than WENO. In addition the hybrid compact-WENO method needs fewer points than the WENO technique to achieve better accuracy in all curves and

ETNA
Kent State University
http://etna.math.kent.edu

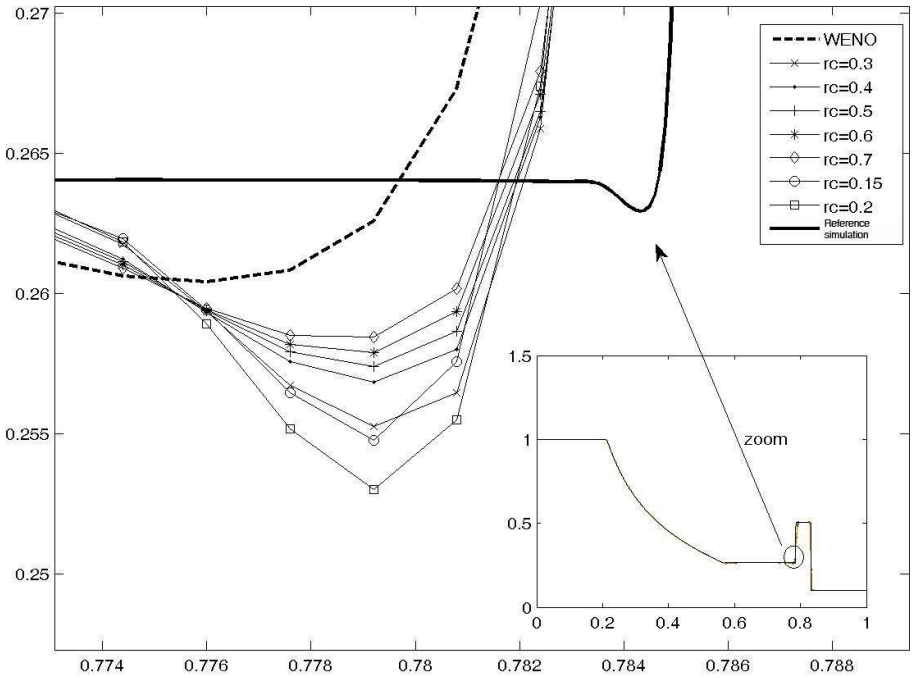

FIGURE 4.2. *Several $\tilde{r}_c$ for problem 2 with 625 points.*

TABLE 4.5
Schemes: Hybrid and WENO for problem 3 in 1D with $N = 625$ points, $T = 0.4$, $\frac{\Delta t}{\Delta x} = 0.8$.

HYBRID	$\tilde{r}_c$	CPU-Time(s)	$\|\|\|_2$	$\|\|\|_\infty$	Local error	% WENO
	0.15	44	0.1179	1.456	0.4407	4.63
	0.2	44.3	0.1190	1.4079	0.4447	5.22
	0.3	44.62	0.1219	1.4874	0.4557	5.83
	0.7	45	0.1290	1.6329	0.4761	8.09
WENO	–	53.7	0.1465	1.7936	0.5496	100

TABLE 4.6
Schemes: Hybrid and WENO for problem 3 in 1D with $N = 1250$ points, $T = 0.4$, $\frac{\Delta t}{\Delta x} = 0.8$.

HYBRID	$\tilde{r}_c$	CPU-Time(s)	$\|\|\|_2$	$\|\|\|_\infty$	Local error	% WENO
	0.15	178	0.0676	1.567	0.1971	5.28
	0.2	178.8	0.0705	1.6507	0.2067	5.97
	0.3	179	0.0727	1.79	0.2034	7.13
	0.7	180	0.0779	1.938	0.2191	10.6
WENO	–	218	0.0876	2.1423	0.2525	100

fewer oscillations in the solution. This can be appreciated in Figures 4.3 and 4.4.

4.2. 2D. PROBLEM 4.4. The first problem consists of a square $[0, 1]^2$, where initially there is a uniformly distributed gas with $\Gamma = \frac{5}{3}$ whose density is everywhere given by

ETNA
Kent State University
http://etna.math.kent.edu

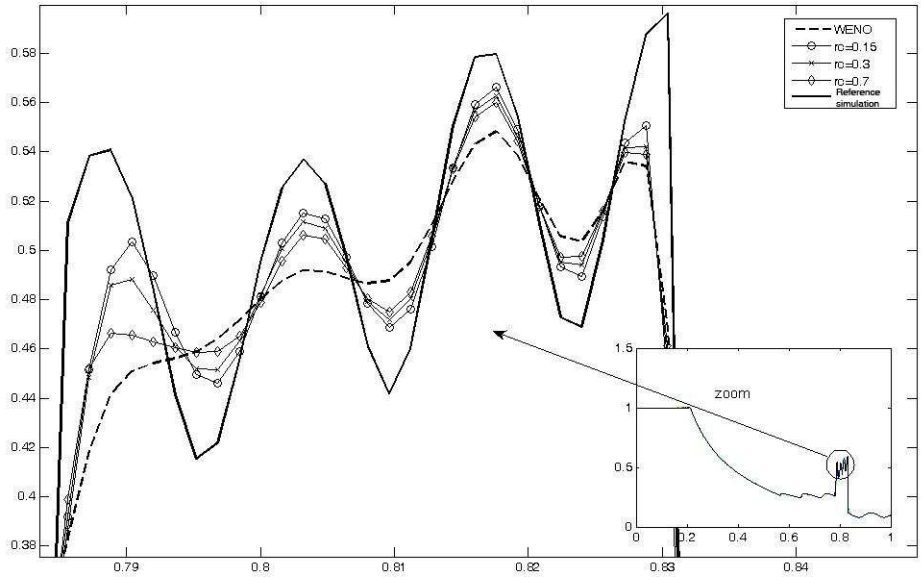

FIGURE 4.3. *Oscilations from the problem* 3 *with* 625 *points.*

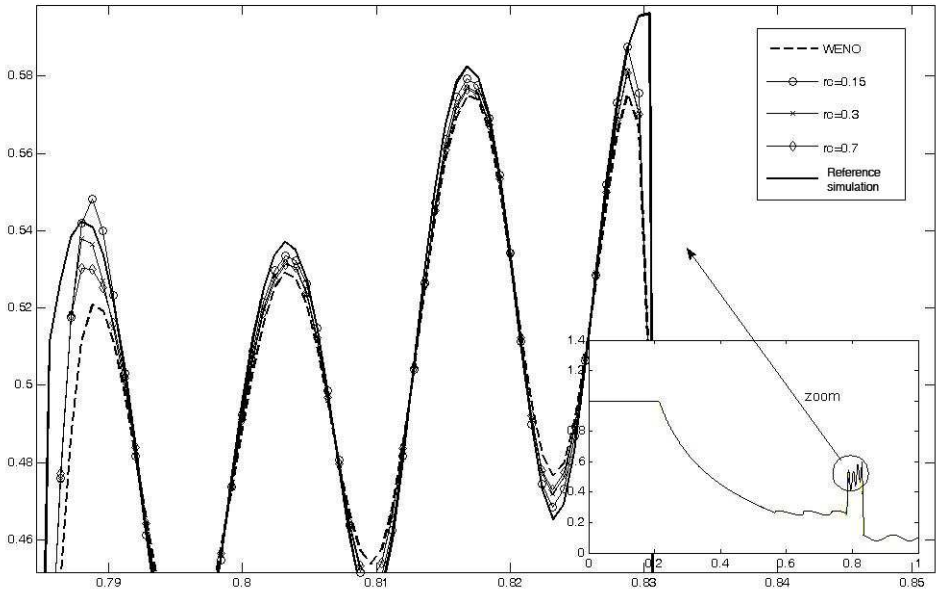

FIGURE 4.4. *Oscilations from the problem* 3 *with* 1250 *points.*

$\rho(0,x,y) = \rho_0 = 10$, $v_0^x(0,x,y) = v_0^x = 0$, $v_0^y(0,x,y) = v_0^y = 0$, and $p = 13.3$ for all x, y. At $t = 0$, an inflow flux is injected into the square with the features: $\rho_0 = 10$, $v_0^x = 0$, $v_0^y = 0.9c$, $p = 13.3$ from the region $0.4 < x < 0.6, y = 0$, while other boundary conditions are set to be absorbent.

ETNA
Kent State University
http://etna.math.kent.edu

Throughout this section, the approximation error is computed with the following formula: supposing u is the exact solution, U its approximation, and N the dimension, then

$$\frac{\sum_{i=1}^{4} ||u(:,:,i) - U(:,:,i)||_2}{\sqrt{4N^2}}, \tag{4.7}$$

where $i = 1, 2, 3, 4$ denotes the number of equations. The results are shown in Tables 4.7 and 4.8, where we can see that the hybrid compact-WENO method has smaller error and smaller execution time than WENO, similarly to what we have seen in 1D. We can appreciate the differences between the algorithms, for example, in the oscillations at the bottom of Figures 4.5 and 4.6.

TABLE 4.7
Schemes for problem 1 in 2D: Hybrid $\left(\frac{\Delta t}{\Delta x} = 0.5\right)$, *WENO* $\left(\frac{\Delta t}{\Delta x} = 0.5\right)$, $N \times N = 125 \times 125$ *points,* $T = 0.8$, $v_0^y = 0.9c$.

HYBRID	$\tilde{r}_c$	CPU-Time (s)	ERROR	% WENO
	0.2	–	–	–
	0.3	1408	10.2821	15.75
	0.5	1444	11.0893	19.86
	0.8	1477	11.4797	25.73
WENO	–	1853	12.6638	100

TABLE 4.8
Schemes for problem 1 in 2D: Hybrid $\left(\frac{\Delta t}{\Delta x} = 0.5\right)$, *WENO* $\left(\frac{\Delta t}{\Delta x} = 0.5\right)$, $N \times N = 250 \times 250$ *points,* $T = 0.8$, $v_0^y = 0.9c$.

HYBRID	$\tilde{r}_c$	CPU-Time (s)	ERROR	% WENO
	0.2	–	–	–
	0.3	8508	5.7804	9.56
	0.5	11088	6.4827	12.71
	0.8	11135	7.0383	18
WENO	–	15279	8.1697	100

PROBLEM 4.5. The second problem has the same features as the previous one except that in this case $v_0^y = 0.99c$. The results are shown in Tables 4.9 and 4.10.

TABLE 4.9
Schemes for problem 2 in 2D: Hybrid $\left(\frac{\Delta t}{\Delta x} = 0.3\right)$, *WENO* $\left(\frac{\Delta t}{\Delta x} = 0.5\right)$, $N \times N = 125 \times 125$ *points,* $T = 0.8$, $v_0^y = 0.99c$.

HYBRID	$\tilde{r}_c$	CPU-Time (s)	ERROR	% WENO
	0.8	2005	91.1982	26.49
	0.85	2015	90.8966	27.54
	0.9	2021	91.4507	28.76
WENO	–	1689	102.4160	100

In this problem, it is important to remark that we have decreased the relation $\frac{\Delta t}{\Delta x}$ to allow the hybrid compact-WENO to work, whereas the WENO works as well as before with $\frac{\Delta t}{\Delta x} = 0.5$. This explains why the hybrid scheme was slower than WENO in the second problem. Nevertheless, the error obtained by the hybrid method is still smaller than the error

ETNA
Kent State University
http://etna.math.kent.edu

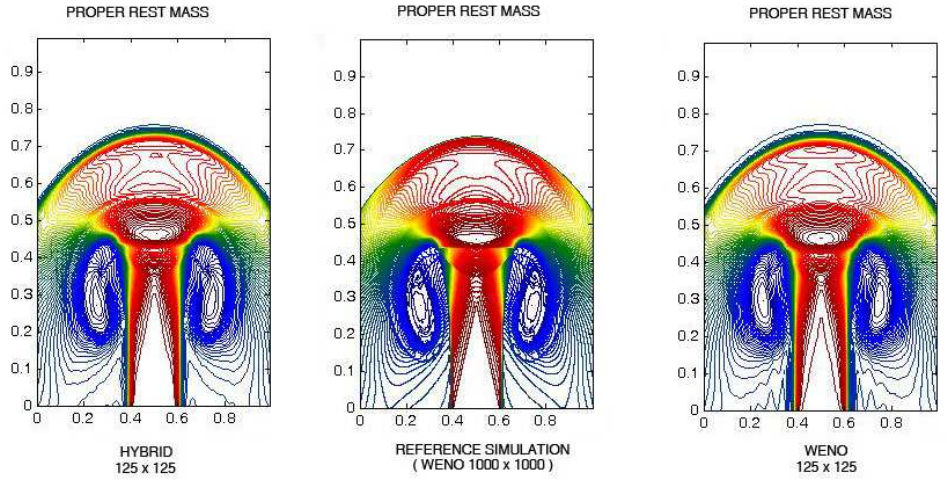

FIGURE 4.5. *Comparative density ρ between hybrid compact-WENO ($\lambda = 0.5$, $\tilde{r}_c = 0.3$) and WENO ($\lambda = 0.5$) for the first problem with 125×125 points.*

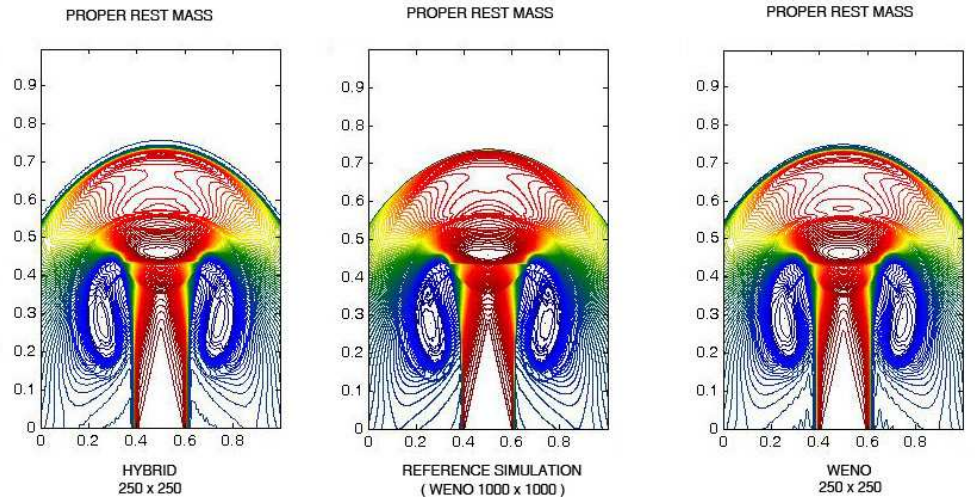

FIGURE 4.6. *Comparative density ρ between hybrid compact-WENO ($\lambda = 0.5$, $\tilde{r}_c = 0.3$) and WENO ($\lambda = 0.5$) for the first problem with 250×250 points.*

TABLE 4.10
Schemes for problem 2 in 2D: Hybrid $\left(\frac{\Delta t}{\Delta x} = 0.3\right)$, WENO $\left(\frac{\Delta t}{\Delta x} = 0.5\right)$, $N \times N = 250 \times 250$ points, $T = 0.8$, $v_0^y = 0.99c$.

HYBRID	$\tilde{r}_c$	CPU-Time (s)	ERROR	% WENO
	0.8	14990	52.1531	18.25
	0.85	15190	52.3219	19.31
	0.9	16609	52.8164	20.61
WENO	–	14034	62.5234	100

ETNA
Kent State University
http://etna.math.kent.edu

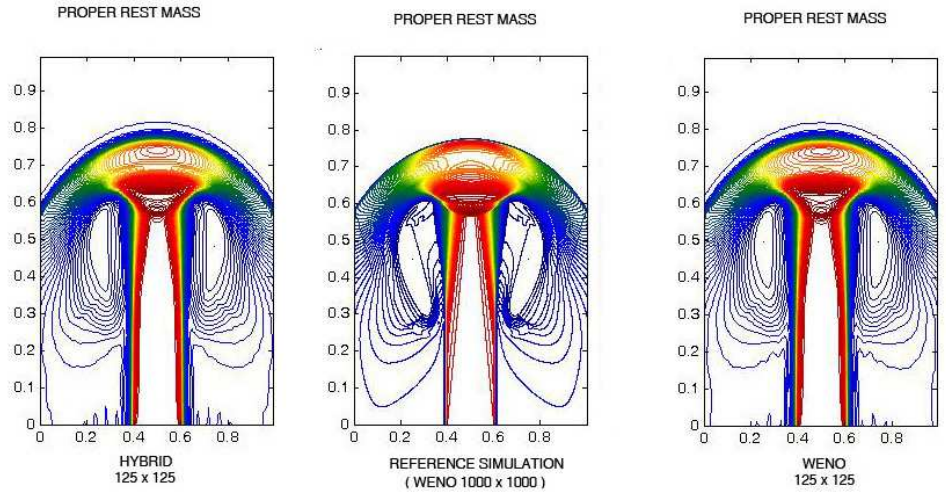

FIGURE 4.7. *Comparative density ρ between hybrid compact-WENO ($\lambda = 0.3$, $\tilde{r}_c = 0.85$) and WENO ($\lambda = 0.5$) for the second problem with 125×125 points.*

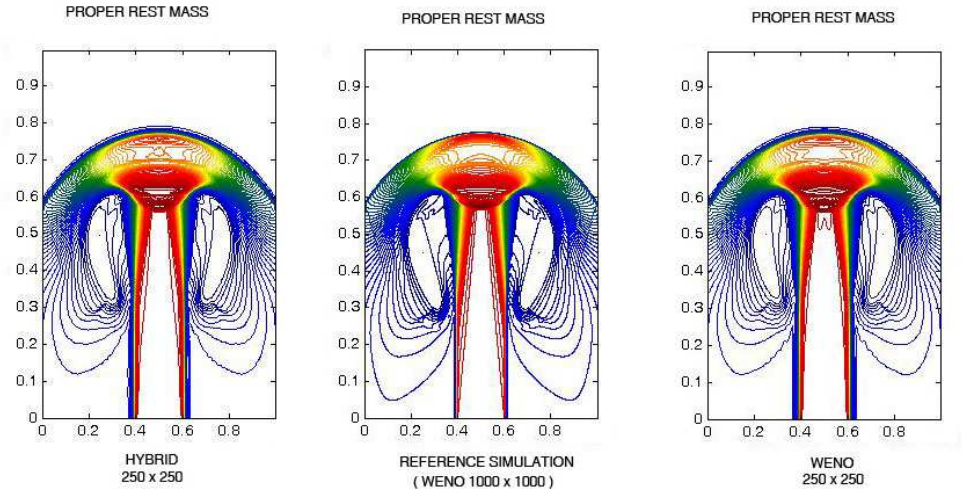

FIGURE 4.8. *Comparative density ρ between hybrid compact-WENO ($\lambda = 0.3$, $\tilde{r}_c = 0.8$) and WENO ($\lambda = 0.5$) for the second problem with 250×250 points.*

obtained by WENO with the same number of points. We can see this in Tables 4.9 and 4.10. In Figures 4.7 and 4.8, we can see how the hybrid scheme decreases the noise at the bottom of the figure. Note also that in Figure 4.8, the hybrid scheme does not have the hump around coordinates ($x = 0.5$, $y = 0.5$) that can be seen in the WENO results.

5. Conclusions. In this article, we have modified the hybrid compact-WENO method proposed in [13] so that it can accurately solve problems with relativistic flows, which are characterized by having strong shocks and turbulence and which therefore have a wide range of scales. More precisely, we numerically illustrated the superiority of the modified hybrid compact-WENO method over the WENO technique for the solution of RFD problems.

In Section 3, we have reviewed in detail the hybrid method of [13] and significant mod-

ETNA
Kent State University
http://etna.math.kent.edu

ifications were introduced to the scheme. In particular, we discussed and reformulated the parameter which determines the behavior of the hybrid scheme in such a way that it can accurately solve the RFD problem; see Section 3.3.

In Section 4, several experiments in 1D and 2D have been carried out to compare the two methods for relativistic problems, including a smooth solution for the 1D case, and we were able to show that the hybrid method gives, as was to be expected, a better resolution in 1D and 2D, owing to its spectral-like resolution property. The 2D experiments were performed for a $v_0^y = 0.99c$.

It is worth pointing out that we have tried to use the hybrid method for the 2D problem (Problem 4.5) with $v_0^y = 0.999c$; however, the results were not satisfactory. It is clear that further modifications are necessary in this case and current work is in progress in this direction.

Acknowledgments. We wish to thank the referees for their valuable comments, which greatly improved this work.

REFERENCES

[1] N. A. ADAMS AND K. SHARIFF, *A high-resolution hybrid compact-ENO scheme for shock-turbulence interaction problems*, J. Comput. Phys., 127 (1996), p. 27.
[2] A. M. ANILE, *Relativistic fluids and magneto-fluids with applications in astrophysics and plasma physics*, Cambridge Monographs on Mathematical Physics, Cambridge University Press, Cambridge, 1989.
[3] B. COCKBURN AND C.-W. SHU, *Nonlineary stable compact schemes for shock calulations*, SIAM J. Numer. Anal., 31 (1994), pp. 607–627.
[4] X. DENG AND H. ZHANG, *Developing high-order weighted compact nonlinear schemes*, J. Comput. Phys., 165 (2000), pp. 22–44.
[5] R. DONAT, J. A. FONT, J. M. IBÁÑEZ, AND A. MARQUINA, *A flux-split algorithm applied to relativistic flows*, J. Comput. Phys., (1998), pp. 58–81.
[6] O. DÖNMEZ, *Solving 1-D special relativistic hydrodynamics (SRH) equations using different numerical methods and results from different test problems*, Appl. Math. Comput., 181 (2006), pp. 256–270.
[7] J. M. IBAÑEZ, *Riemann solvers in relativistic hydrodynamics: Basics and astrophysical applications*, Journal of Korean Astronomical Society, 34 (2001), pp. 191–201.
[8] G.-S. JIANG AND C.-W. SHU, *Efficient implementation of weighted ENO schemes*, J. Comput. Phys., 126 (1996), pp. 202–228.
[9] S. K. LELE, *Compact finite defference schemes with spectral-like resolution*, J. Comput. Phys., 103 (1992), pp. 16–42.
[10] J. M. MARTÍ AND E. MÜLLER, *Numerical hydrodynamics in special relativity*, Living Rev. Relativ., 6 (2003). Available at http://www.livingreviews.org/lrr-2003-7.
[11] M. L. NORMAN AND K.-H. A. WINKLER, *Why ultrarelativistic numerical hydrodynamics is difficult*, in Astrophysical Radiation Hydrodynamics, K.-H. A. Winkler and M. L. Norman, eds., NATO ASI Series C, 188, Reidel, Dordrecht, Netherlands, 1986, pp. 449–475.
[12] S. PIROZZOLI, *Conservative hybrid compact-WENO schemes for shock-turbulence interaction*, J. Comput. Phys., 178 (2002), pp. 81–117.
[13] Y.-X. REN, M. LIU, AND H. ZHANG, *A characteristic-wise hybrid compact-WENO scheme for solving hyperbolic conservation laws*, J. Comput. Phys., (2003), pp. 365–386.
[14] C. SHU, *Essentially non-oscillatory and weighted essentially non-oscillatory schemes for hyperbolic conservation laws*, in Advanced Numerical Approximation of Nonlinear Hyperbolic Equations, B. Cockburn, C. Johnson, and C.-W. Shu, eds., Springer, Berlin, 1998, pp. 325–432.
[15] S. ZHANG, S. JIANG, AND C.-W. SHU, *Development of nonlinear weighted compact schemes with increasingly higher order accuracy*, J. Comput. Phys., 227 (2008), pp. 7294–7321.